JJMIE

Volume 16, Number 1, January. 2022
ISSN 1995-6665
Pages 105 - 111

Jordan Journal of Mechanical and Industrial Engineering

Design of Multi Joint Integrated Control System for Non Driven Robot

Qian Zhang *

Department of Computer Science, Guangdong University of Education, Guangzhou 510303, China

Received 14 July 2021 *Accepted 29 December 2021*

Abstract

All joints of the non-driving robot have driving devices, but they can not be controlled effectively, which increases the difficulty of the robot control. In order to solve this problem, a multi joint integrated control system for non- actuated robot is designed in this paper. The research object is a two-degree of freedom non-actuated robot. After designing the basic structure of the robot, the dynamic characteristics of the robot are analyzed, and the integrated control system is designed from two aspects of current and position. The experimental results show that the design method can realize the accurate motion control of multi- joints of non-driven robot, which provides a reference for practical application.

Keywords: Non driven robot; Joint control; Integrated control system;

1. Introduction

Because the joint of ordinary robot is controlled and driven separately, the activity is relatively simple, while the actual control input of non-driven robot is less than the motion freedom of the robot, the underactuated part is generally set at the end of the robot. Compared with the conventional series robot, it has many advantages, such as light weight, small inertia, simple structure design and low system cost [1-3]. At the same time, the end joint of the non driven robot is driven by the cooperative action of multiple joints, so the fault tolerance rate of the non-driven robot is relatively high [4]. The robot with the number of independent control inputs less than the actual motion degree of freedom has good flexibility and light weight, and can be applied to some extreme environments. Therefore, the non-driven robot has always been one of the important fields of robot research. Wang et al. studied the multi arm concentric tube robot. The concentric tube robot has the advantages of small volume and strong shape control ability, which improves the shortcomings of most single arm robots. A four-degree of freedom vision arm and two six-degree of freedom mechanical arms are designed, and the end effector of CTR system is configured at the end to enable the robot to realize surgical operation, however, the positioning and tracking effect of control is general [5]. Wang et al. mainly studied the timed formation control of multi robot systems with time-delay constraints. Through the state transformation of the predictor to deal with the input delay caused by the network connection, a nonlinear fixed time formation protocol is proposed, and the corresponding stability time is calculated by Lyapunov function to realize the effective control of the robot, but the balance control effect of the driving arm is general [6]. Liu et al. studied the multi-objective control system based on DOB. The stability of the characteristic equation with uncertain time delay is analyzed by using the zero exclusion criterion, and the anti-interference performance and robustness of the system are studied. In the presence of uncertain time delay and disturbance, effective control is realized, but the response effect of the control system is poor [7]. Based on the above research, the design method proposed in this paper solves the problem of difficult motion control of non drive system. The control effect of the designed control system is studied, which provides a preliminary reference for the multi joint control of non driven robot.

2. Model Construction of 2-DOF Non Driven Robot

In the non driving robot system, the joints without driving ability can only be controlled by the driving joints, so the position control method is much more difficult than the general full driving system. In this paper, a multi joint robot is designed, which has one driving joint and one non-driving joint. The structure is relatively simple and has the basic characteristics of underactuated system. It is an ideal research object for us to study the multi joint integrated control problem of non driven robot.

2.1. Performance index of robot system

The planar 2-DOF robot has two parallel rotating joints, and the second joint is a non driving joint. Its main parameters and performance indicators are shown in Table 1.

* Corresponding author e-mail: zhqian020@126.com.

Table 1 Main parameters and performance indexes of robot

Freedom	2	DD motor drive + encoder
Structural form	Planar joint type	Encoder + brake
Base size (support foot)	1500 mm × 1500 mm	Unlimited rotation
Height	1350 mm	Torque control
Motion plane	The angle with the horizontal plane is 60 degrees	PC computer + motor driver
Arm length (wheelbase of two joints)	340 mm	

2.2. Mechanical structure design of robot

The structure of the first degree of freedom is shown in Figure 1.

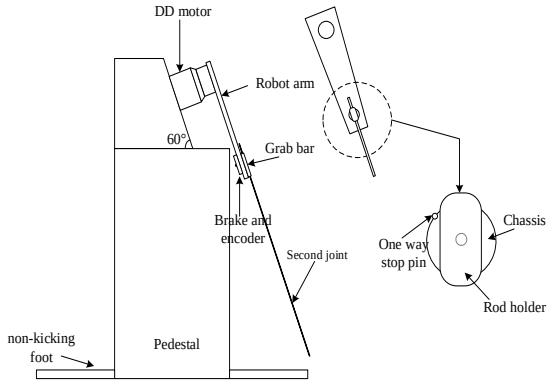

Figure 1. Structure of robot

Base and support foot: The base is the coordinate reference of robot motion, so it is necessary to keep the stability and balance of the base under the high-speed motion of robot arm. Since the reaction force of the arm to the base is quite large during the high-speed swing, a heavy block is added to the base to increase the stability (as shown in Figure 1). Meanwhile, the deployable support foot is designed to increase the support area and prevent the robot from overturning.

The first joint: driven by a DD motor. In our research, the control method is to give the driving torque directly to control the robot torque. In order to improve the control accuracy and reaction speed, the direct drive motor is used. The actual maximum output torque of the motor is 110 nm, which is limited to 100 nm in our experiment.

The second joint is a non-driving joint. In this joint, an encoder is used to measure the joint motion angle, and a brake device is used to provide the braking force after the action. A one-way stop pin is set on the joint of the robot to block the excessive clockwise rotation angle of the grab rod.

2.3. Kinematics equation of robot

The $x-y$ coordinate is established with the motion plane of robot arm as the coordinate plane, and the axis of the first joint is used as the coordinate origin. θ_1 and θ_2 are defined as the motion angles of the first joint and the second joint. Then the forward kinematics solution of the grab bar is as follows:

$$\begin{cases} x = l_1 \cos\theta_1 + l_2 \cos(\theta_1 + \theta_2) \\ y = l_1 \sin\theta_1 + l_2 \sin(\theta_1 + \theta_2) \end{cases} \quad (1)$$

l_1 and l_2 are the length of two connecting rods, l_1 is the distance from the axis of the first joint to the axis of the second joint, and the measured value is 0.34 M; l_2 is the distance from the axis of the second joint to the target point [8].

The inverse kinematics solution is as follows:

$$\begin{cases} \theta_1 = \arctan\left(\dfrac{(l_1 + l_2\cos\theta_2)y - l_2 x \sin\theta_2}{l_2 y \sin\theta_2 + (l_1 + l_2\cos\theta_2)x}\right) \\ \theta_2 = \arccos\left(\dfrac{x^2 + y^2 - l_1^{\,2} - l_2^{\,2}}{2l_1 l_2}\right) \end{cases} \quad (2)$$

According to the different arm shape, there are multiple solutions, that is, there are positive and negative solutions when solving θ_2 in the above equation.

2.4. Bottom control structure of robot

Since only one drive joint needs motor control, the underlying control hardware of the robot is relatively simple. However, since the grab bar action is a high-speed motion, the whole process only takes about 0.8 seconds, and there are complex torque changes in this process, so the requirements for the performance of the underlying hardware are also very high [9-12].

The hardware structure of the control system is shown in Figure 2.

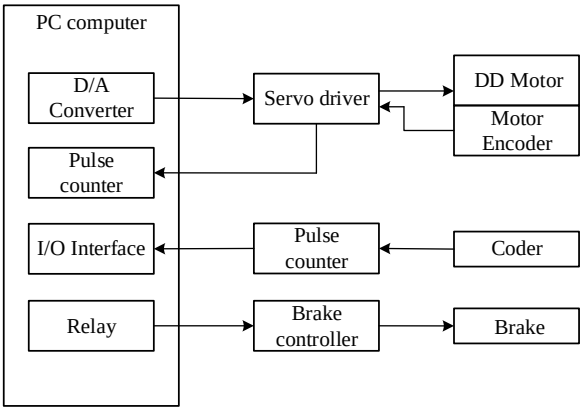

Figure 2 Robot control hardware

The control computer is nec pc-9801 microcomputer with DOS 6.0 operating system. The D / a converter converts the calculated control torque into analog quantity and outputs it to the motor driver to drive the motor to move. At the same time, a pulse counter is used to receive the signal of motor code disk. Due to the high precision of code disk of DD motor (319 488 pulses per revolution) and high frequency of code disk signal under high speed operation, qpg45 high-speed pulse counter is used, and the counting frequency can reach 1.8 mhz. For the non driven joint, an encoder is used to feedback the angle of the joint, and the brake is used for braking. The encoder signal is

read through the I/O interface of the computer after counting, and the brake is controlled by the computer through the relay. The reaction time of braking is 50 ms for braking, 20 ms for releasing braking, and the braking torque is 25 nm.

The sampling period of the whole control is 1 millisecond, and the timing interrupt is provided by 8 253 chip. In the bottom control, the current loop (torque) is controlled by the motor driver, and the speed loop and position loop are controlled by the computer in software mode, that is, the PID controller of software servo [13-16]. Since the non-driving joint has no control torque, the PID controller has two inputs and one output, that is to adjust the two joints at the same time. In fact, it is equivalent to the superposition of the output of the two PID controllers. The effect is Equation (3):

$$u = K_{p1}\Delta\theta_1 + K_{I1}\int\Delta\theta_1 + K_{d1}\Delta\dot{\theta}_1 + K_{p2}\Delta\theta_2 + K_{I2}\int\Delta\theta_2 + K_{d2}\Delta\dot{\theta}_2 \quad (3)$$

The coefficients are adjusted according to the experimental results. As explained in the introduction of the first chapter, such PID feedback controller can not guarantee the uniform convergence of the error. In fact, in the process of motion, the effect of the two joint errors on the controller will cancel each other. However, it can keep the balance between the errors of two joints, prevent one-sided increase of the error of one joint, and can effectively reduce the error when the effect of two joint errors is the same.

The control structure of the whole system is shown in Figure 3, in which the track generation part is calculated off-line, and the calculated track data is transmitted to the lower computer for the bottom control as a file. The lower computer controls the robot to complete the action. The dynamic feedforward + PID feedback control is used in the control. The feedforward control signal is the torque track calculated off-line. The PID controller is realized by the software of the lower computer. The motion track calculated offline is used as the reference signal of PID regulation.

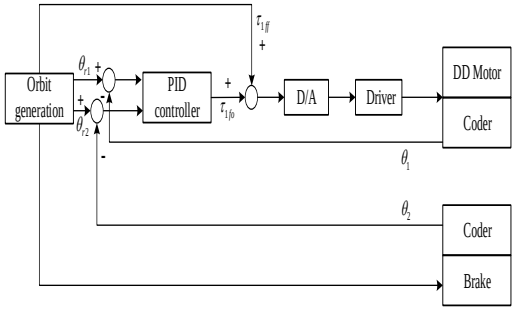

Figure 3. Overall control structure of robot

3. Design of Robot Integrated Control System

Based on the analysis of robot dynamics, the robot integrated control system is designed from two aspects: current controller and position controller. Differential feedforward and fuzzy control are introduced to improve the response effect of system position.

3.1. Design of current controller

The current controller consists of four parts: current feedback, PI controller, three-phase inverter and motor stator armature circuit. Its main function is to improve the rapidity of the system and suppress the internal interference of the current loop [17]. According to the overall block diagram of the system introduced in Section 2.3, the current loop consists of two non-interference loops, torque current i_q and excitation current i_d. In this paper, the control methods of the two loops are identical, so the design of torque current i_q loop is only introduced.

The current loop control loop is shown in Figure 4. $H(s)$, $G_p(s)$, $G_s(s)$ and $G_s(s)$ represent the transfer functions of current feedback, PI controller, three-phase inverter and motor stator armature circuit respectively.

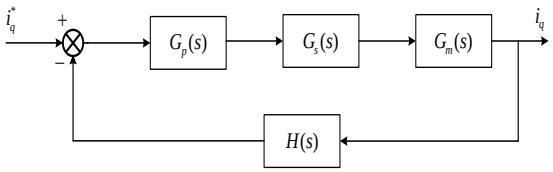

Figure 4. Current loop control loop

The current feedback link can be divided into three parts: detection, filtering and sampling. The detection part can be regarded as a proportion link. The filter is a hardware implemented RC filter, which can be regarded as a first-order inertial link, and its transfer function is $G_{RC}(s) = \frac{1}{RCs+1} = \frac{1}{\tau_{RC}s+1}$. Among them, $\tau_{RC} = RC$ is the time constant of RC filter circuit. The sampling part is realized by ad module in the controller, and its transfer function is $G_{AD}(s) = \frac{1}{\tau_{AD}s+1}$. Therefore, the transfer function of the current feedback link can be expressed as follows:

$$H(s) = K_1 G_{RC}(s) G_{AD}(s) G_s(s) = \frac{1}{(\tau_{AD}s+1)(\tau_{RC}s+1)}$$

Because τ_{AD} and τ_{RC} are relatively small, they can be replaced by a first-order inertial link with a time constant τ_{fb}. Equation (4) can be simplified as follows:

$$H(s) \approx \frac{K_1}{\tau_{fb}s+1} \quad (5)$$

Among them, $\tau_{fb} = \tau_{AD} + \tau_{RC}$ and K_1 are the magnification of the detection link.

The three-phase inverter can be regarded as an amplifier, which can amplify the output signal of the front current PI controller to the voltage signal of the direct control motor. However, due to the output delay of SVPWM algorithm, the delay is at least half of the PWM switching cycle. Therefore, the transfer function of the three-phase inverter can also be regarded as a first-order inertial link. The transfer function can be expressed as follows:

$$G_s(s)=\frac{K_2}{\tau_{pwm}s+1} \tag{6}$$

Among them, τ_{pwm} is half of PWM switching period and K_2 is voltage amplification factor of three-phase inverter.

The stator armature of the motor has stator resistance R_m and stator inductance L_m, which can be regarded as the first-order inertial link. The transfer function is as follows:

$$G_m(s)=\frac{1}{R_m(\tau_L s+1)} \tag{7}$$

where $\tau_L=\frac{L_m}{R_m}$ is the time constant of stator armature inductance.

The transfer function of PI controller can be expressed as follows:

$$G_p(s)=K_p+\frac{K_i}{s}=\frac{K_p(\tau_i s+1)}{\tau_i s} \tag{8}$$

K_p and K_i are the proportional constant and integral constant of PI controller respectively.

Figure 4 open loop transfer function of current loop can be expressed as follows:

$$G_i(s)=\frac{K_pK_1K_2(\tau_i s+1)}{R_m\tau_i s(\tau_{fb}s+1)(\tau_{pwm}s+1)(\tau_L s+1)} \tag{9}$$

Since the inductance time constant τ_L is generally much larger than the current feedback link time constant τ_{fb} and PWM switching period τ_{pwm}, the zero point and large time constant pole cancellation of the current regulator are selected:

$$\tau_i=\tau_L=\frac{L_m}{R_m} \tag{10}$$

Therefore, Equation (9) can be simplified as follows:

$$G_i(s)=\frac{K}{s(\tau_{fb}s+1)(\tau_{pwm}s+1)} \tag{11}$$

Among $K=\frac{K_pK_1K_2}{L_m}$.

The time constant τ_{fb} and switching period τ_{pwm} of the current feedback link are relatively small, so an inertial link can be used to replace the two inertial links, $\tau=\tau_{pwm}+\tau_{fb}$. Equation (11) is further simplified:

$$G_i(s)=\frac{K}{s(\tau s+1)} \tag{12}$$

The closed-loop transfer function of the current controller is a typical second-order system:

$$G_i(s)=\frac{G_i(s)}{1+G_i(s)}=\frac{K/\tau}{s^2+s/\tau+K/\tau} \tag{13}$$

By comparing the standard form of closed-loop transfer function of current controller, the damping coefficient ζ and undamped natural frequency ω_n can be obtained:

$$\begin{cases}\omega_n=\sqrt{\frac{K}{\tau}}\\ \zeta=\frac{1}{2\tau\omega_n}=\frac{1}{2}\sqrt{\frac{1}{K\tau}}\end{cases} \tag{14}$$

According to the characteristics of the second-order system, the damping coefficient is inversely proportional to the overshoot. When the damping coefficient is large, the overshoot of the system is small, but the response speed is slow; The smaller the damping coefficient, the greater the overshoot, but the faster the response speed. Therefore, it is necessary to select the damping coefficient ζ of the system reasonably. From the engineering test, $\zeta=0.707$ is the optimal index of the second-order system, so $K=1/2\tau$ can be obtained. The proportional constant K_p and integral constant K_i of PI controller are obtained:

$$\begin{cases}K_p=\frac{L_m}{2\tau K_1K_2}\\ K_i=\frac{R_m}{2\tau K_1K_2}\end{cases} \tag{15}$$

3.2. Design of position controller

People are most concerned about whether the robot arm can quickly and accurately move to the preset position. Therefore, in the design of the control algorithm of the joint servo driver, the design of the position controller is the most important. The control parameters of traditional PID controller have been fixed, which can only have the best control effect for one or several working conditions, and can not respond to the external real-time changes. Therefore, this paper introduces the fuzzy PID control algorithm in the design of position controller. In the design of position control algorithm, the most taboo is that the position control appears overshoot and static error. On the basis of fuzzy PID control algorithm, the differential feed-forward link is added to eliminate the overshoot of the control system.

3.2.1. Controller design based on Fuzzy PID algorithm

Fuzzy control theory is a kind of control theory based on language rules and fuzzy reasoning based on fuzzy set theory in modern control theory. Its mathematical basis is fuzzy set theory, which belongs to an important branch of intelligent control. The structure of fuzzy PID controller is shown in Figure 5. The fuzzy controller with two inputs and three outputs is adopted. The input is the error between the position feedback signal and the given quantity and the error change rate. The output is the three parameters ΔK_p, ΔK_i and ΔK_d of PID controller.

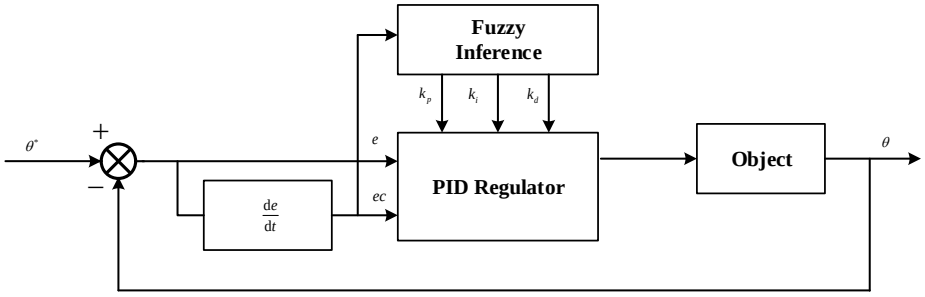

Figure 5 Schematic diagram of fuzzy PID

Firstly, the input signals E and EC, the output signals ΔK_p, ΔK_i, ΔK_d are transformed into fuzzy variables for input into fuzzy inference engine for processing. The input signal and output signal are divided into seven levels, corresponding to seven fuzzy subsets {positive big (PB), positive middle (PM), positive small (PS), zero (Zo), negative small (NS), negative medium (nm), negative large (NB)}. The fuzzy universe covering the input signal and the output signal is set as {-6, -5, -4, -3, -2, -1, 0, 1, 2, 3, 4, 5, 6}, and the input and output signals obey the triangular membership function.

Secondly, since the position servo system is not allowed to be out of calibration and overshoot, special attention should be paid to the adjustment of integral coefficient K_i in the process of adjustment. When the system error is large, the larger K_p and the smaller K_i and K_d should be selected to make the system response have better fast tracking performance and avoid integral saturation and large overshoot. When the system error is small, in order to make the system have good steady-state performance, K_i should be appropriately increased, but attention should be paid not to make the system overshoot.

Finally, the output of fuzzy reasoning is defuzzified, and the method of maximum membership degree is usually used, that is to select the domain element with the largest membership degree in the output fuzzy set as the judgment result. Finally, the calculation equation of three PID parameters is as follows:

$$K_p = K_{p0} + \Delta K_p \tag{16}$$

$$K_i = K_{i0} + \Delta K_i \tag{17}$$

$$K_d = K_{d0} + \Delta K_d \tag{18}$$

where, is the initial value of PID, is the output of fuzzy controller.

3.2.2. Design of differential feedforward controller

The position loop control system is composed of position controller, speed closed loop and permanent magnet synchronous motor. Since the cut-off frequency of the position loop is far less than the reciprocal of each time constant of the speed loop, the speed loop is approximately equivalent to the first-order inertial link $G_v(s) = \frac{k_v}{T_n s + 1}$, and the permanent magnet synchronous motor is approximately equivalent to the integral link $G_m(s) = \frac{k_m}{s}$. The feed-forward control structure diagram of the position loop is shown in Figure 6.

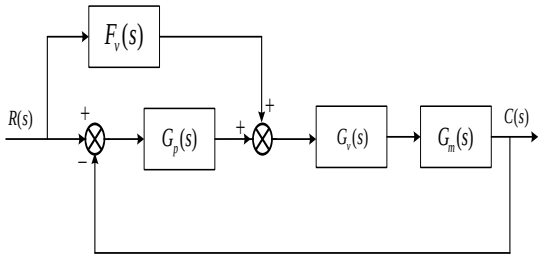

Figure 6. Structure diagram of position loop feedforward control

The closed-loop transfer function of the system is obtained from the structure diagram of position loop feedforward control:

$$\frac{C(s)}{R(s)} = \frac{\left[F_v(s) + G_p(s)\right] G_v(s) G_m(s)}{1 + G_p(s) G_v(s) G_m(s)} \tag{19}$$

From Equation (19), it can be concluded that:

$$F_v(s) = \frac{1}{G_v(s) G_m(s)} = \frac{s(T_n s + 1)}{k_v k_m} \tag{20}$$

The transient error and steady-state error of the system are both zero. Since the accuracy of the servo system depends on the low frequency part of the system, the high-order part in the equation can be ignored and simplified as follows:

$$F_v(s) = \frac{s}{k_v k_m} \tag{21}$$

In other words, the feedforward of the position loop is the differential of the given position, and the speed can be predicted according to the given position, and the predicted value can be compensated to the given speed so as to realize the early response.

4. Experimental Part

Matlab/Simulink is used for simulation experiment. The experimental system is windows 10, equipped with Core i7 processor and 8 g memory, which can meet the experimental requirements. Assuming that the initial angle of the non driving arm is $\theta_{20} = 0.8\left[rad\right]$ and the initial angular velocity is $\dot{\theta}_{20} = 0\left[rad/s\right]$, the expected points to be achieved by the control are: angle $\theta_{2d} = 0.5\left[rad\right]$, angular velocity $\dot{\theta}_{2d} = 0\left[rad/s\right]$.

4.1. Balance control test of drive arm

The initial angular velocity of the active arm and underactuated arm is 0, the maximum simulation step size is 1 ms, and the simulation time is 5 s. Test the free swing angle value of the active arm and underactuated arm near the vertical downward stable equilibrium position, as shown in Figure 7.

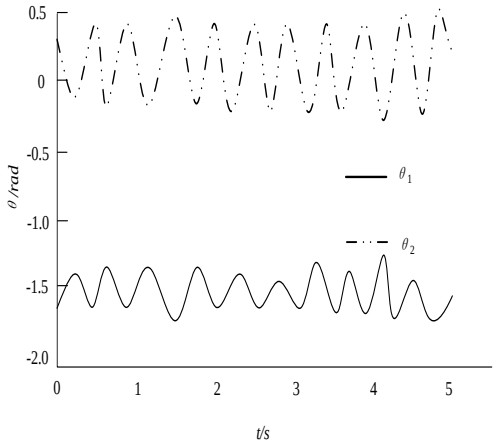

Figure 7. Free swing range of active arm and underactuated arm

By changing the position input parameters, balance control is carried out near the vertical unstable equilibrium position, and the balance control of the first joint and the second joint is tested. The experimental results are shown in Figure 8.

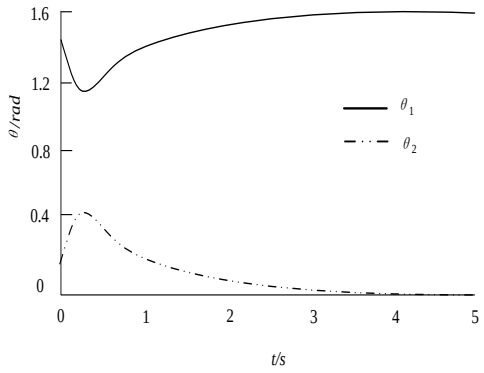

Figure 8. Angle value (LQR)

It can be seen from Figure 8 that the angle θ_1 of the active arm (the first joint) approaches π/2, and the angle θ_2 of the underactuated arm (the second joint) approaches to 0, which proves that the design method can be used for balance control.

4.2. Given position tracking test

A sine wave with an amplitude of 20° and a frequency of 1 Hz is given. The response of the control method in Reference [5] and Reference [6] and the control method designed in this paper are compared respectively, as shown in Figure 9.

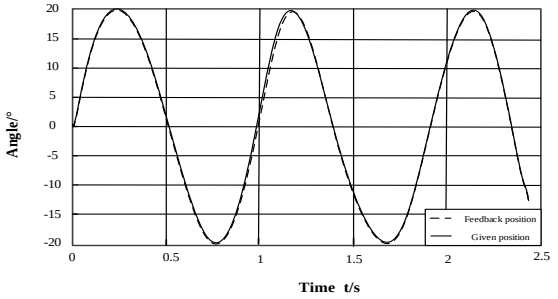

(a) The method of this paper

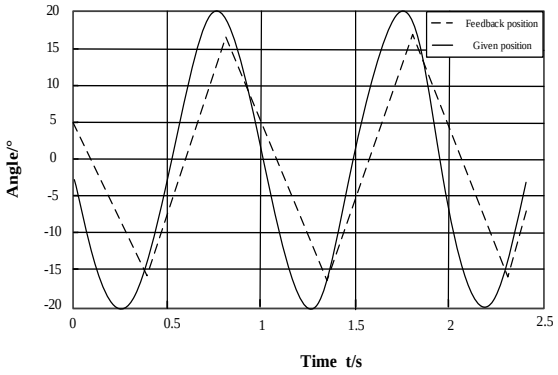

(b) Method of Reference [5]

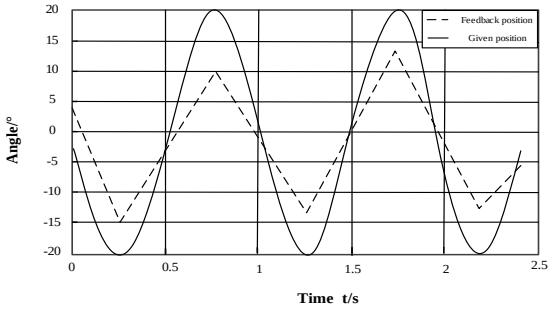

(c) Method of Reference [6]

Figure 9 Experimental results of given position tracking

From the observation of Figure 9, it can be seen that when the position is given as a real-time sine wave, the proposed method can track the given position well and has good dynamic response performance. However, the method in the literature has poor performance in tracking the given position with real-time changes. Therefore, the proposed method has good practical performance.

5. Conclusions

In order to solve the problem that the non-actuated joints can not be well controlled in the non-actuated robot system, a multi-joint integrated control system of the non-actuated robot is designed in this paper. Differential feedforward and fuzzy control are introduced to improve the response effect of the system position. Experiments show that the system designed in this paper can track the given position well. Additionally, the experiments also show that the effect of balance control is good, and good results are obtained. The system designed in this paper can solve some problems existing in the motion control of non-driving system. Such system has good applicability to the comprehensive control of non-driving multi joints, which

realizes accurate motion control of non-driving robot multi joints, and can also provide a scientific basis for non-driving robot to participate in more work.

Acknowledgements

The research is supported by: Computer Experimental Teaching Demonstrating Center (undergraduate teaching quality and teaching reform project of Guangdong education); Guangdong University of Education Network Engineering Key Subject (No. ZD2017004); The undergraduate teaching quality and teaching reform project of Guangdong University of Education (Experimental Teaching Demonstration Center of Computer Application) (No. 2018sfzx01).

References

[1] Kim, Y.J.; Park, S.W.; Yeom, H.G.; Bang, M.S.; Kim, J.S.; Chung, S.K.; Kim, S. A study on a robot arm driven by three-dimensional trajectories predicted from non-invasive neural signals. Biomedical Engineering Online, 2015, 14: 81.

[2] Rijk, R.D.; Rushton, M.; Khajepour, A. Out-of-plane vibration control of a planar cable-driven parallel robot using a multi-axis reaction system. IEEE/ASME Transactions on Mechatronics, 2018, (4): 1-1.

[3] Park, H.; Hutchinson, S. Robust rendezvous for multi-robot system with random node failures: An optimization approach. Autonomous Robots, 2018, 42(8): 1807-1818.

[4] Zhi, Z.; Huan, Z.; Swanson, A.R.; Weitlauf, A.S.; Warren, Z.E.; Sarkar, N. Design, development, and evaluation of a noninvasive autonomous robot-mediated joint attention intervention system for young children with ASD. IEEE Transactions on Human-Machine Systems, 2018, 48(2): 125-135.

[5] Wang, J.; Yang, X.; Li, P.; Song, S.; Liu, L.; Meng, M.Q.H. Design of a multi-arm concentric-tube robot system for transnasal surgery. Medical & Biological Engineering & Computing, 2020, 58(3): 497-508.

[6] Wang, C.Y.; Tnunay, H.; Zuo, Z.Y.; Lennox, B.; Ding, Z.T. Fixed-time formation control of multirobot systems: Design and experiments. IEEE Transactions on Industrial Electronics, 2019, 66(8): 6292-6301.

[7] Liu, Q.; Liu, M.; Jin, Q.B.; Liu, Y.J. Design of DOB-based control system in the presence of uncertain delays for low-order processes. IEEE Transactions on Control Systems Technology, 2020, 28(2): 558-565.

[8] Kasmuri, N.H.; Kamarudin, S.K.; Abdullah, S.R.S.; Hasan, H.A.; Som, A.M. Integrated advanced nonlinear neural network-simulink control system for production of bio-methanol from sugar cane bagasse via pyrolysis. Energy, 2019, 168: 261-272.

[9] Mutawe, S.; Hayajneh, M.; BaniHani, S.; Qaderi, M.A. Simulation of trajectory tracking and motion coordination for heterogeneous multi-robots system. Jordan Journal of Mechanical and Industrial Engineering, 2021, 15(4): 337-345.

[10] Chen, Y.F.; Zhao, H.C.; Mao, J.; Chirarattananon, P.; Helbling, E.F.; Hyun, N.S.P.; Clarke, D.R.; Wood, R.J. Controlled flight of a microrobot powered by soft artificial muscles. Nature, 2019, 575(7782): 324-329.

[11] Dong, C.Y.; Yang, S.F.; Jia, H.J.; Wang, P. Padé-based stability analysis for a modular multilevel converter considering the time delay in the digital control system. IEEE Transactions on Industrial Electronics, 2019, 66(7): 5242-5253.

[12] Kong, F.X.; Zhu, Y.H.; Yang, C.; Jin, H.Z.; Cai, H.G. Integrated locomotion and deformation of a magnetic soft robot: Modeling, control and experiments. IEEE Transactions on Industrial Electronics, 2021, 68(6): 5078-5087.

[13] Koyama, K.; Shimojo, M.; Ming, A.; Ishikawa, M. Integrated control of a multiple-degree-of-freedom hand and arm using a reactive architecture based on high-speed proximity sensing. The International Journal of Robotics Research, 2019, 38(14): 1717-1750.

[14] Yang, C.G.; Jiang, Y.M.; He, W.; Na, J. Adaptive parameter estimation and control design for robot manipulators with finite-time convergence. IEEE Transactions on Industrial Electronics, 2018, 65(99): 8112-8123.

[15] Hashlamon, I. Adaptive disturbance estimation and compensation for delta robots. Jordan Journal of Mechanical and Industrial Engineering, 2020, 14(4): 413-422.

[16] Li, S.H.; He, H.Y.; Dong, K.F.; Sheng, L.X. Research on real-time integrated control method of PV-SHAPWH. Solar Energy, 2019, 182: 213-224.

[17] Derakhshani, A. On the uncertainty analysis of uplift capacity of suction caissons in clay based on the fuzzy sets theory. Ocean Engineering, 2018, 170: 416-425.